CrossMark

Teleconnected influence of tropical Northwest Pacific sea surface temperature on interannual variability of autumn precipitation in Southwest China

Lin Wang · Wen Chen · Wen Zhou · Gang Huang

Abstract The interannual variation of autumn precipitation in Southwest China (SWC) and the possible influence of tropical Northwest Pacific (NWP) sea surface temperature (SST) are investigated. Statistical analysis shows that SWC precipitation is negatively correlated with concurrent NWP SST. The warm NWP SST that promotes dry conditions in SWC is linked to three dynamical processes: (1) Warm NWP SST excites an anomalous cyclone over the South China Sea, which is oriented against the climatological flow, weakening the transportation of moisture from the NWP. (2) Warm NWP SST strengthens the westerlies along the equatorial Indian Ocean. As a result, most of the moisture is transported over the maritime continent and thus the poleward flow carrying moisture from the Indian Ocean into SWC becomes weaker. (3) Warm NWP SST provokes anomalous ascent and upper-level divergence in situ, with one path of the outflow heading northwestward and converging over SWC, which induces compensating subsidence over the SWC region. The results of numerical experiments, forced by SST anomalies in the NWP alone, are found to reproduce the observed atmospheric response, indicating that the impact of NWP SST on SWC precipitation is physical and that the moisture conditions over SWC are triggered primarily by the fluctuation of NWP SST. Due to the persistent SST anomaly over NWP from summer to autumn, the NWP SST in the preceding summer can be considered a predictor for autumn drought in SWC. Furthermore, autumn precipitation in SWC has experienced a significant decrease since 1994, probably maintained by the long-lasting warm NWP SST in recent decades.

Keywords Drought · Precipitation · Southwest China · Northwest Pacific · SST

L. Wang
Key Laboratory of Regional Climate-Environment for Temperate
East Asia, Institute of Atmospheric Physics, Chinese Academy
of Sciences, Beijing 100029, China

W. Chen (✉)
Center for Monsoon System Research, Institute of Atmospheric
Physics, Chinese Academy of Sciences, Beijing 100190, China
e-mail: chenw@mail.iap.ac.cn

W. Zhou
Guy Carpenter Asia-Pacific Climate Impact Centre, School
of Energy and Environment, City University of Hong Kong,
Hong Kong, China

G. Huang
State Key Laboratory of Numerical Modeling for Atmospheric
Sciences and Geophysical Fluid Dynamics, Institute
of Atmospheric Physics, Chinese Academy of Sciences,
Beijing 100029, China

G. Huang
Joint Center for Global Change Studies, Beijing 100875, China

1 Introduction

In recent decades, frequent severe and sustained droughts have hit Southwest China (SWC), and those that occurred in the summer of 2006 (Li et al. 2009), the autumn of 2009 to the spring of 2010 (Yang et al. 2012), and the late summer of 2011 broke 50-year records. According to statistics reported by the Chinese government (http://english.gov.cn/index.htm), severe drought in conjunction with high temperatures in the summer of 2006 brought drinking water shortages to at least 18 million residents, caused total crop failure on 311,300 hectares, and caused total economic losses estimated at 11.74 billion yuan. During the once-in-a-century drought that emerged in the autumn of 2009 and persisted into the subsequent spring of 2010, more than 16 million people and 11 million livestock did not have

adequate access to drinking water, with a direct economic loss of 19 billion yuan. Similarly, the drought in the late summer of 2011 affected a combined 5.86 million hectares of crops, leaving a total of 9.17 million livestock and 12 million people short of drinking water. All of these catastrophic droughts constitute devastating and far-reaching threats to agriculture, water availability, ecosystems (Zhang et al. 2012a, b), the economy, and society (Ye et al. 2012). Besides the oppressive heat waves and lack of effective precipitation, the complex topography, erosion, deforestation, and poor water management exacerbated the worst drought events in SWC (Qiu 2010).

Before the occurrence of the severe 2006 summer drought over SWC, drought-related research focused mainly on eastern China and its associated summer and winter monsoon (Chen et al. 2009, 2013a, b; Huang 2004; Zhou et al. 2012, 2006; Zhou and Chan 2006; Wang et al. 2013). During recent years, devastating droughts in SWC have received widespread attention from both the Chinese government and the academic sector. For instance, Zhang et al. (2013a) investigated drought characteristics in SWC during the last 50–100 years. In parallel, much effort has been dedicated to determining the atmospheric circulation mechanism responsible for causing these three droughts. For the 2006 summer drought, as suggested by Li et al. (2009), the westward shift and intensification of the Western Pacific subtropical high (WPSH) and the northward shift of the midlatitude westerlies were both unfavorable for precipitation in SWC. For the prolonged drought from the autumn of 2009 until the spring of 2010, an extremely negative phase of the Arctic Oscillation played an important role in bringing the track of cold air invasion eastward, leading to weakened convergence of warm moist air from the south and cold dry air from the north (Barriopedro et al. 2012; Yang et al. 2012). Moreover, Lu et al. (2011) pointed out that the persistent warm temperatures during 2009–2010 also contributed to the drought in SWC, because high temperature makes it hard for the air to become saturated. In addition, Zhang et al. (2013b) discussed the possible influence of El Niño Modoki on the 2009 autumn drought over SWC.

Despite significant drought research in SWC, there are no studies dealing with the common atmospheric and oceanic conditions related to drought events. Consequently, we need to move beyond case study findings toward a more general survey. More recently, Feng et al. (2014) discussed the cause of severe droughts over SWC in the dry season (January–February–March) during 1951–2010 and concluded that circulation anomalies are generated by remote forcing from the tropical Pacific and North Atlantic Oceans. Their work was not limited to the 2010 event but uncovered the mechanism responsible for all dry events with a magnitude comparable to that of the 2010 case.

In this study, we endeavor to reveal the cause of rainfall variability in SWC in autumn (September–October–November) at an interannual timescale. Autumn is a season of transition between summer (rainy season, >150 mm month^{-1}) and winter (dry season, <20 mm month^{-1}), so a significant reduction of autumn precipitation will inevitably lead to sustained and enhanced drought. Therefore, a discussion of precipitation variation in SWC during autumn has fundamental implications. Moreover, the aforementioned studies are based on statistical techniques and do not actually describe a cause-and-effect relationship. To overcome this problem, in this study we carry out a series of numerical experiments to better understand the physical mechanism and to verify the results from statistical analysis.

The rest of the paper is structured as follows: The data, methods, and model are described in Sect. 2. The influences of tropical Northwest Pacific (NWP) SST on the precipitation variability in SWC at the interannual timescale are examined in Sect. 3. Finally, conclusions and a discussion are presented in Sects. 4 and 5, respectively.

2 Data, methods, and model

The monthly precipitation observations used in this study are a gridded dataset that has $0.5° \times 0.5°$ horizontal grids and covers the period from 1961 to 2011, compiled by the National Meteorological Information Center of the China Meteorological Administration. The atmospheric data, with a horizontal resolution of $1.25°$ by $1.25°$, including vertically integrated moisture flux and vertical velocity, both of which play a crucial role in the development of precipitation (Li et al. 2012, 2013), are obtained from the Japanese 55-year reanalysis (JRA-55), which is a newly released reanalysis product provided by the Japan Meteorological Agency (Ebita et al. 2011). Sea surface temperature (SST) data on a $2° \times 2°$ grid are retrieved from the NOAA extended reconstruction sea surface temperature (ERSST; Smith et al. 2008). Note that all data are restricted to the period from 1961 to 2011.

The observation-based analysis is conducted based on linear techniques such as correlation, regression, and composite analysis. The Atmospheric General Circulation Model (AGCM) used is the Community Atmosphere Model version 5.1 (CAM5.1), which was released as a part of the Community Earth System Model (CESM). In this study, we use the finite volume dynamic core at a horizontal resolution of $1.9°$ latitude and $2.5°$ longitude with 30 vertical levels (hybrid pressure-sigma vertical coordinate). The relevant information about CAM5.1 can be found at http://www.cesm.ucar.edu/. Figure 1 illustrates the location of SWC on a map of China. SWC covers Chongqing, Sichuan, Guizhou, Yunnan, and west of Guangxi.

Fig. 1 Location of Southwest China (*top left*) and its topography (*bottom right*, units: m)
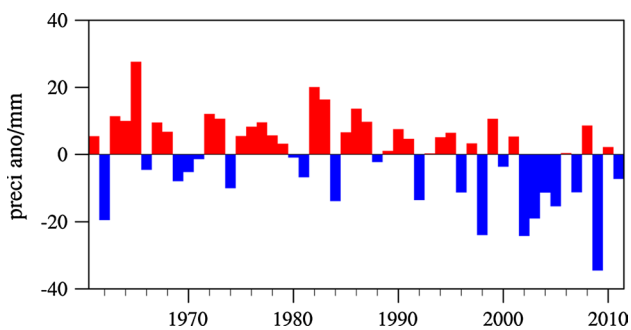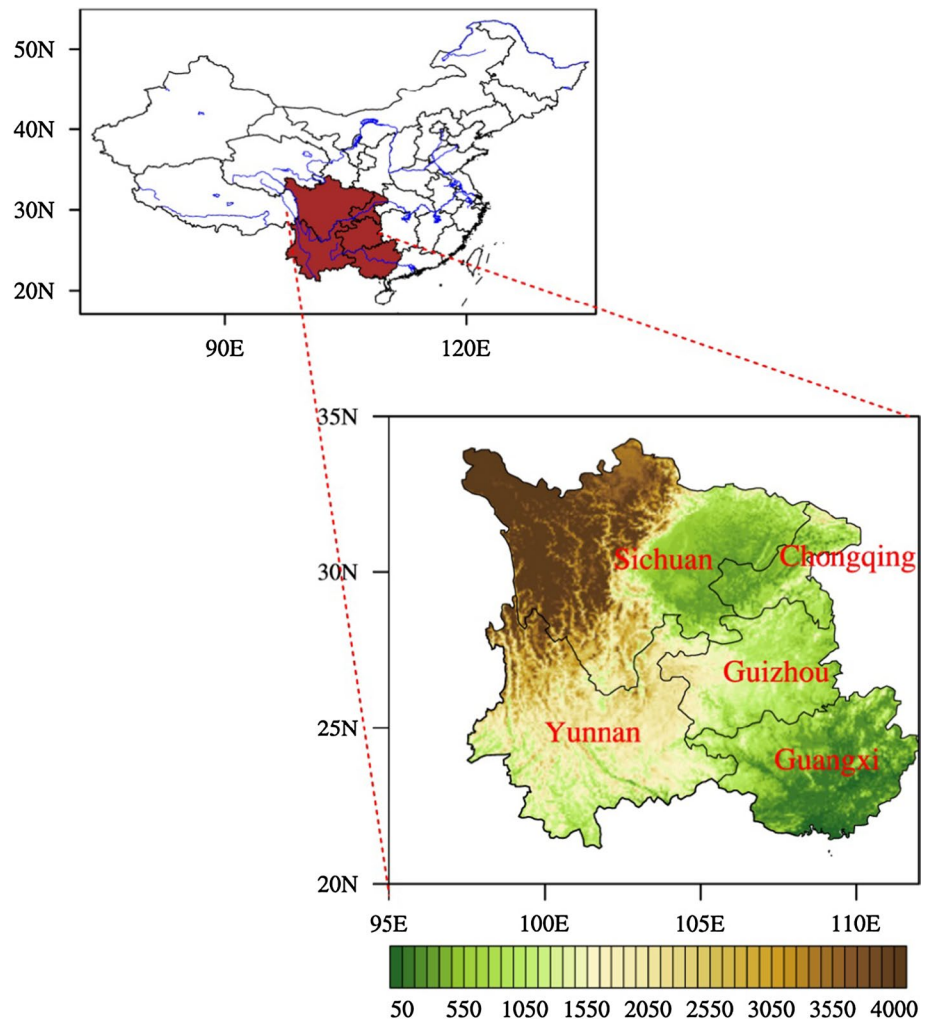

Fig. 2 Interannual variation of SWC precipitation departures from 1961 to 2011. Reference period is 1961–2011

3 Results

3.1 Interannual variation of precipitation in SWC and its statistical relation with SST

Figure 2 shows the interannual variation of the autumn precipitation in SWC from 1961 to 2011. There is a clear

downward trend with a linear rate of about −0.32 mm a^{-1}, which is significant at the 99 % confidence level. This implies that precipitation in SWC has decreased by 16 mm over the last 51 years. Besides the long-term trend, SWC precipitation also exhibits multidecadal change, with an abrupt change in 1994, after which the precipitation remains overall below average. Here, the turning point is detected by the Mann–Kendall mutation test (figure not shown).

Figure 3 maps the correlation between the area-averaged precipitation in SWC and grid-point SST from summer to autumn on an interannual timescale. As shown in the simultaneous correlation map (Fig. 3b), the SWC autumn precipitation is highly correlated with the SST in the NWP (0–18°N, 120–160°E), with correlation coefficients (CC) of up to −0.5. The relationship is such that the SWC precipitation responds negatively to warmer SST anomalies in the NWP. As indicated by previous studies, thermal condition in NWP sector usually has impact on East Asia climate (Shang et al. 2014). It is also noteworthy that a statistically significant negative correlation already exists between autumn SWC precipitation and the NWP SST during the preceding summer (Fig. 3a),
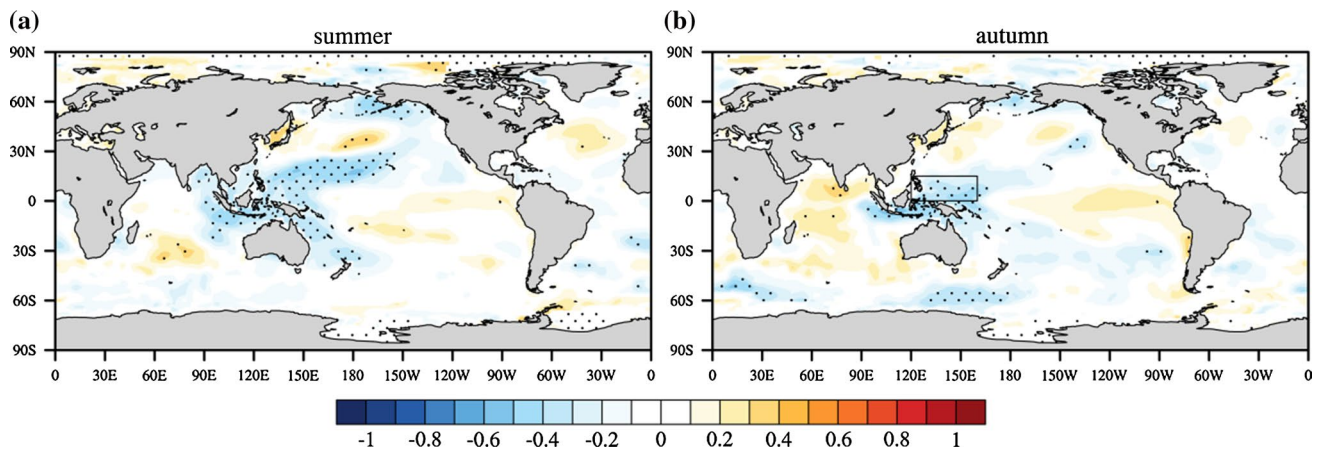
(a)

(b)

Fig. 3 Global distribution of CC between the SWC autumn precipitation and SST of two successive seasons, from preceding summer (**a**) to autumn (**b**), with the stippling denoting correlations exceeding the 95 % confidence level. Prior to calculating CC, both SST and precipitation are high-pass filtered to retain fluctuations on timescales shorter than 10 years
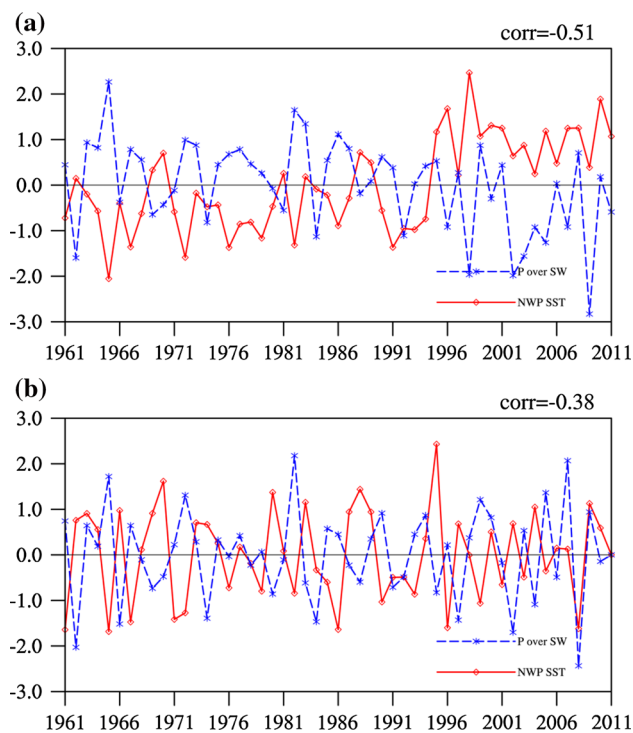
(a)

(b)

Fig. 4 Raw (**a**) and 10-year high-pass-filtered (**b**) time series of standardized SWC precipitation departures (*blue dashes*) and NWP SST departures (*red solid*). Reference period is 1961–2011

Fig. 5 Autumn precipitation anomalies (mm) regressed onto the NWPSSTI. *Stippling* indicates anomalies significant at the 95 % confidence level

suggesting that the NWP SST in summer could be exploited as a forecasting aid (discussed later in Sect. 3.4).

Temporal evolutions of the standardized SWC precipitation and NWP SST for autumn are depicted in Fig. 4a, which once again reveals a simultaneous negative correlation between them (CC = −0.51). The NWP SST also experiences a sudden change in 1994, in accordance with a change in SWC precipitation. After 1994, the standardized NWP SSTs are
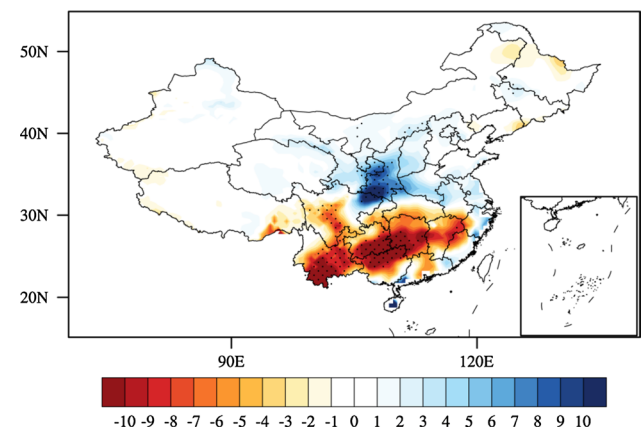
predominantly above one standard deviation. To separate interannual signals, a high-pass filter is applied to eliminate fluctuations with periods longer than 10 years. As seen from Fig. 4b, this filter removes decadal variation as well as long-term trends and keeps interannual variations only, since the slope of SWC precipitation and NWP SST are respectively −0.003 mm a^{-1} and 0.0004 °C a^{-1}, neither of which exceeds the significance level. Moreover, the correlation between high-pass-filtered SWC rainfall and NWP SST is still significant, with a CC equal to −0.38. In addition, an analysis of sliding correlation with a 27-year window (figure not shown) indicates stable teleconnection between NWP SST and SWC precipitation across the whole period (1961–2011). To focus on the interannual variation, therefore, all data are filtered to exclude variation longer than 10 years. Due to the filter edge effects, in addition, the first and last 4 years of the time series are not considered in the following analysis.

3.2 Large-scale circulation features associated with NWP SST anomalies

To facilitate description, the NWP SST index (NWPSSTI) is defined as the normalized SST regionally averaged over the tropical NWP sector (0–18°N, 120–160°E). The spatial pattern of autumn precipitation regressed onto the NWPSSTI is illustrated in Fig. 5. It is noticeable that the most pronounced negative anomalies reaching 10 mm month^{-1} per standard deviation of the NWP SST appear in SWC. Outside the SWC region, in contrast, the regressions show very small values and are statistically insignificant. Therefore, the precipitation deficit in SWC is closely associated with warmer-than-normal NWP SST, which is consistent with the correlation map as displayed in Fig. 3.

Before turning to the examination of large-scale circulation anomalies forced by NWP SST, the climatological pattern of atmospheric circulation in East Asia is first demonstrated. Diagnosis of the climatological mean of the vertically integrated water vapor flux (Fig. 6a) reveals two major pathways of moisture flow into SWC, one from over the NWP that crosses the South China Sea and Indo-China Peninsula and the other from the equatorial Indian Ocean. The change in circulation caused by NWP SST is shown in Fig. 7, in which the NWPSSTI is regressed against vapor flux anomalies. Warmer NWP SST induces an anomalous cyclonic flow over the South China Sea and the surrounding region, which is oriented against the climatological flow and thereby prevents the transfer of moisture from the NWP into SWC. Meanwhile, when NWP SST increases, westerly moisture transport along the equatorial Indian Ocean to Indonesia is reinforced, but the meridional flow that brings moisture from the Bay of Bengal into SWC becomes weaker. Consequently, both of these processes result in decreasing moisture availability and hence an unfavorable environment for the production of precipitation in SWC.

To highlight the atmospheric responses to NWP SST anomalies, composite analysis is conducted to pick out all the strong cases. NWP SST warm and cold events (hereafter warm and cold events for short) are defined as those with NWPSSTI above or below one standard deviation from the mean, respectively. The standard deviation is calculated for the base period 1961–2011. According to this criterion, warm events occur in 1970, 1980, 1983, 1988, 1995, and 2004, while cold events occur in 1965, 1967, 1971, 1972, 1986, 1990, 1996, and 1999. The composite maps of precipitation, moisture transport, and vertical velocity corresponding to warm and cold years are shown in Figs. 8, 9, and 10, respectively. The pattern differences between the composites of warm and cold events are also illustrated. As shown in Fig. 8c, the rainfall during the warm years tends to be 20–30 mm below that during cold
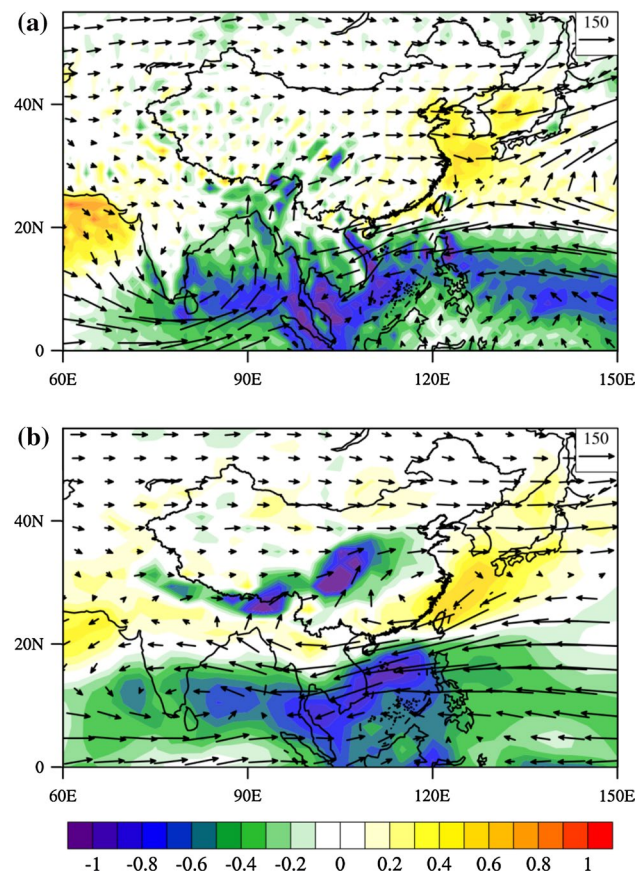

Fig. 6 Climatological patterns of observed (**a**) and model-simulated (**b**) vertically integrated water vapor flux over a depth from the surface to 300 h Pa (*vectors*, in units of kg s^{-1} m^{-1}) and moisture divergence (*shading*, in units of 10^{-4} kg s^{-1} m^{-2}) in East Asia
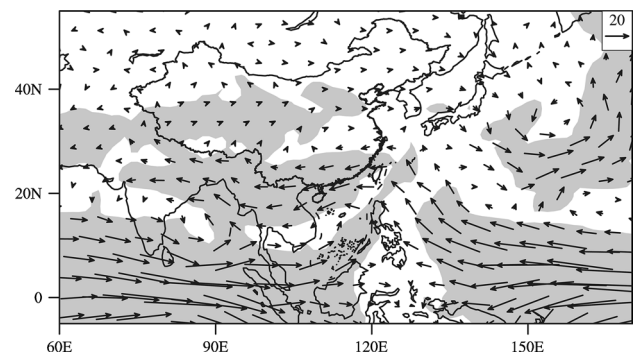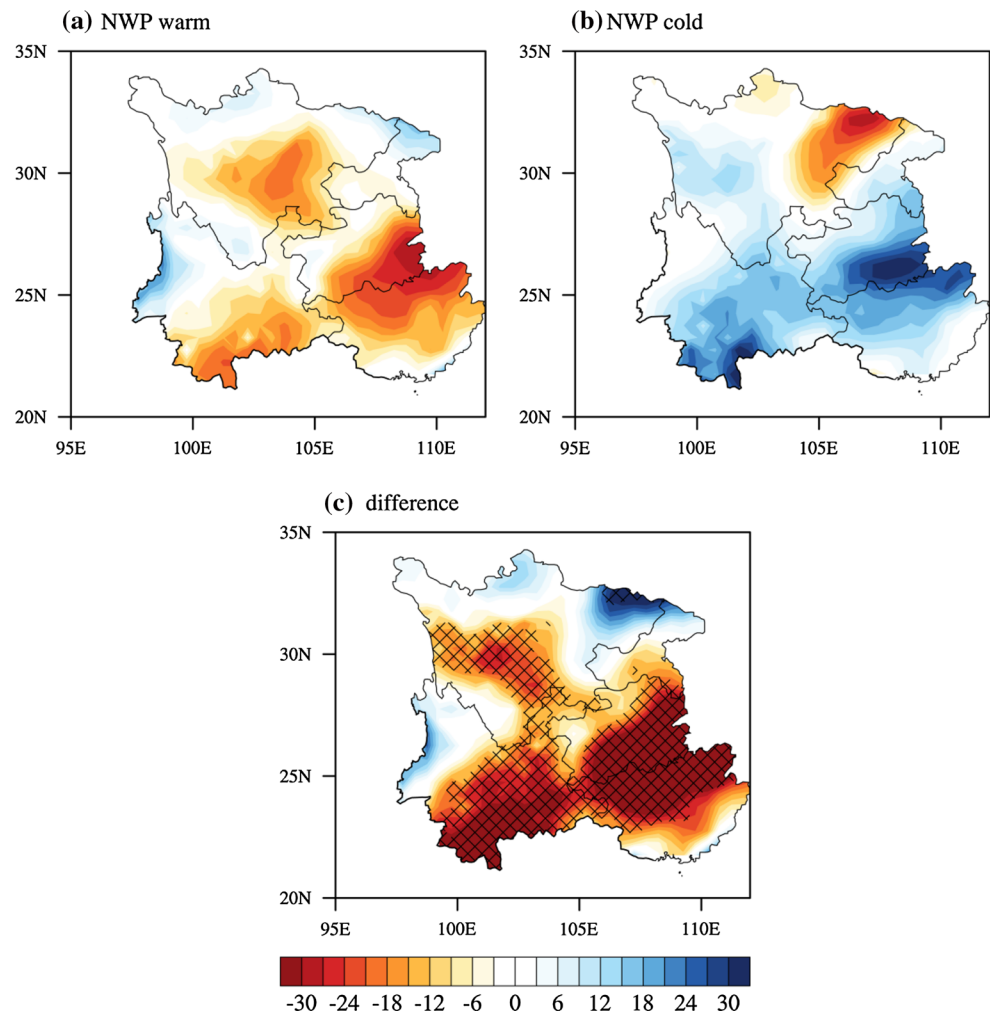

Fig. 7 Regression of NWPSSTI onto vertically integrated water vapor flux. Areas significant at the 95 % confidence level are *shaded*

years in most parts of SWC, with the only exception in east Sichuan. Furthermore, composite precipitation anomalies show opposite signs for warm versus cold events and are similar to the regression outcomes (Fig. 5).

Identical comparisons are made with moisture transport and vertical velocity. The warm-minus-cold

Fig. 8 Composite precipitation anomalies (mm) over SWC for warm (**a**) and cold events (**b**). Composite difference between warm and cold events is shown in (**c**) with *cross hatches* indicating the field significant at the 95 % confidence level

composite of moisture transport and its associated divergence, as shown in Fig. 9c, reveals a cyclonic pattern centered at the South China Sea to the northwest of the warm SST site, which leads to weakened moisture transport from the NWP into SWC. Meanwhile, owing to enhanced westerlies over the equatorial Indian Ocean, the poleward water flux into SWC decreases. Consequently, anomalous water vapor diverges over South China (shaded in Fig. 9), leading to a decrease in moisture availability and precipitation. In contrast, cold NWP SST has the opposite effect on the circulation pattern, which favors moisture transport into SWC.

As seen in Fig. 10, vertical velocity indicates considerable and robust signals in the NWP and SWC. Over the high-SST region, greater updraft velocities result (Fig. 10c), since it is expected that high SST produces warm humid air and low-level wind convergence, which subsequently intensifies the upward motion. The compensating subsiding branch lies in SWC and thus suppresses clouds and rainfall.

3.3 Numerical experiments

To verify the physical rather than statistical significance of the NWP SST on SWC precipitation, AGCM numerical experiments are conducted to isolate the NWP SST-induced circulation anomalies. The control simulation, imposed by the prescribed climatological SST, is integrated for 20 years, with the last 15 years being used for the control climate in the atmospheric model. The control experiment is designated as CTL. In parallel, a sensitivity experiment is performed that is identical to the control except that the SST is raised (referred to as NWP_warm) or decreased (referred to as NWP_cold) by 1 °C uniformly throughout the NWP. For both the warm and cold SST experiments, there are 15 separate members, with each simulation covering the period of 1 Sep to 31 Nov; meanwhile, the 15 ensemble members vary only in atmospheric initial conditions, taken from 1 Sep in the last 15 years of the simulation derived from the control run. In the following, the 15-member ensemble mean in the perturbation experiment minus CTL is presented in order to
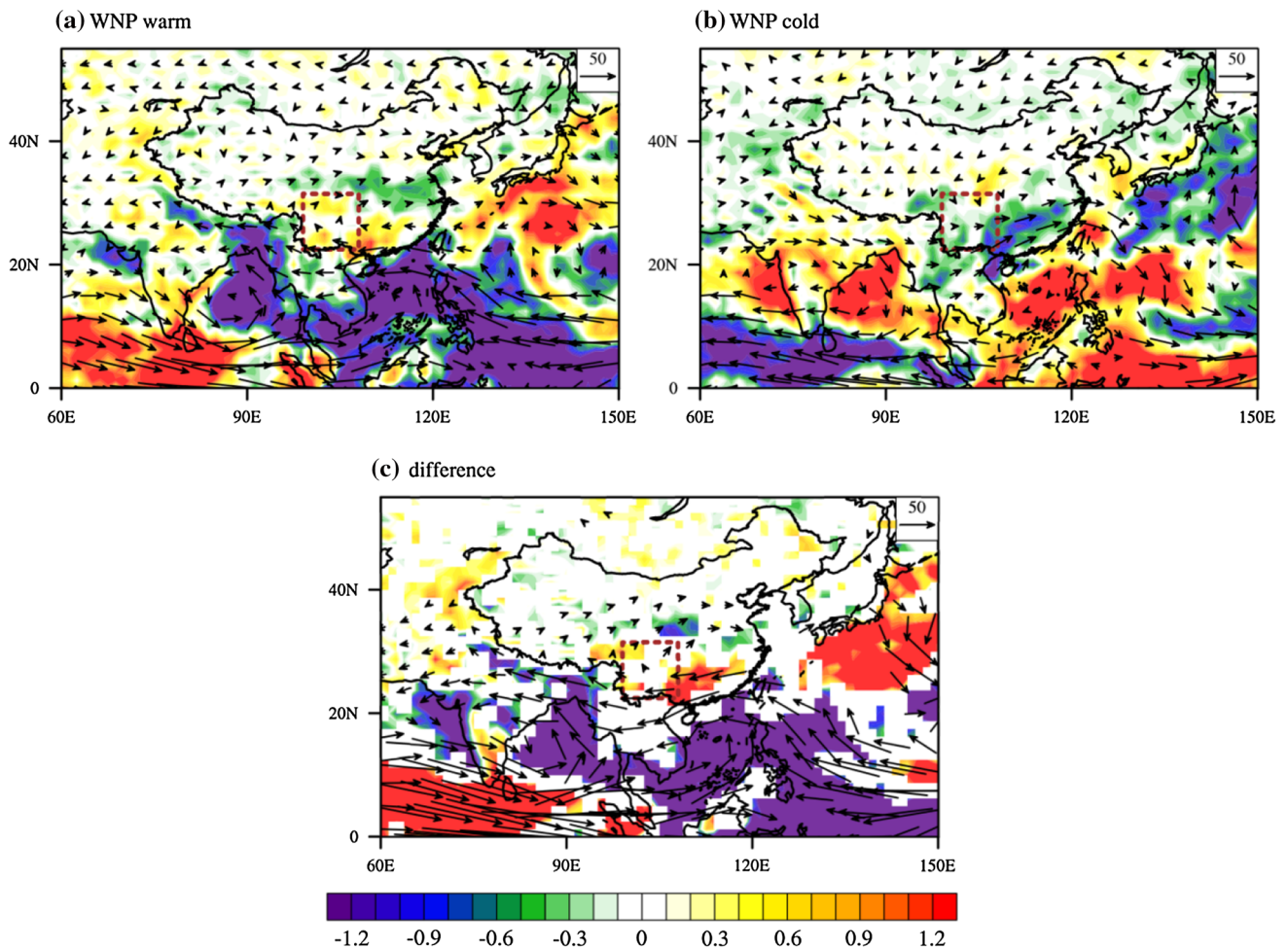
Fig. 9 The same as Fig. 8, but for vertically integrated water vapor flux (*vectors*, in units of kg s^{-1} m^{-1}) and moisture divergence (*shading*, in units of 10^{-5} kg s^{-1} m^{-2}). The *dashed rectangle* marks the SWC region. In subplot (**c**), only values significant at 90 % confidence level are *plotted*

remove the internal variability of the model and highlight the SST-induced anomalous pattern.

The control simulation is evaluated in terms of its ability to reproduce a realistic climate pattern, as shown in Fig. 6b. The control simulation results in reasonable mean states of vertically integrated water vapor flux in East Asia. In particular, CAM5.1 successfully captures the fundamental large-scale features of the two pathways of moisture transport associated with the precipitation in SWC, though the center of cyclonic flow over the Bay of Bengal is shifted slightly westward relative to observed climatology.

Figure 11 portrays the difference in autumn rainfall between the experiment with the warmer/colder NWP SST and the control run with climatological SST. In the warm SST condition, the reduced precipitation centered over SWC reaches a minimum of about −40 mm. When forced by cold NWP SST, in contrast, the AGCM produces excessive rainfall in most parts of SWC. When the NWP

SST is warm, an anomalous cyclone forms in the South China–South China Sea area, which can be interpreted as a consequence of a Gill Mode response to thermal forcing in the tropics (Gill 1980), and the westerly flow over the equatorial Indian Ocean into the maritime continent is strengthened, both of which lead to less moisture transported into SWC and weakened low-level convergence there (shaded in Fig. 12). Since little moisture is available, it is unlikely that precipitation will form (Fig. 11a). However, the cold NWP SST configuration favors increased moisture flow and thereby more precipitation in SWC. It is also noteworthy that the climate responses in the AGCM, in which the SST anomaly is added only within the NWP, closely resemble the major features of the observed composites (Fig. 9), reflecting the critical influence that NWP SST exerts on precipitation fluctuation in SWC. Similar comparisons are made with 500 h Pa vertical velocity and 200 h Pa divergent wind, as shown in Figs. 13 and 14. In
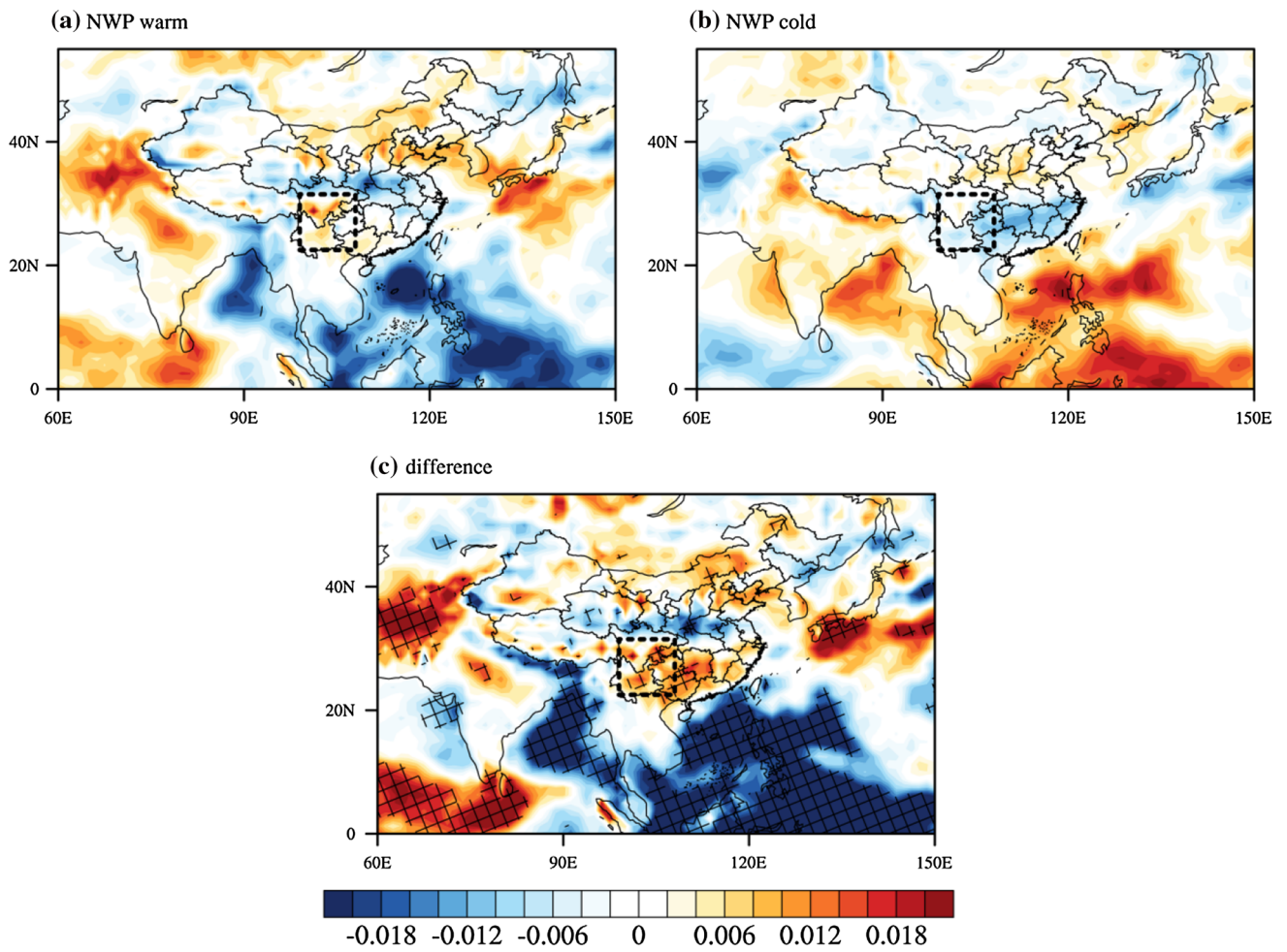
(a) NWP warm

(b) NWP cold

(c) difference

Fig. 10 The same as Fig. 8, but for pressure vertical velocity at 500 h Pa (Pa s^{-1})
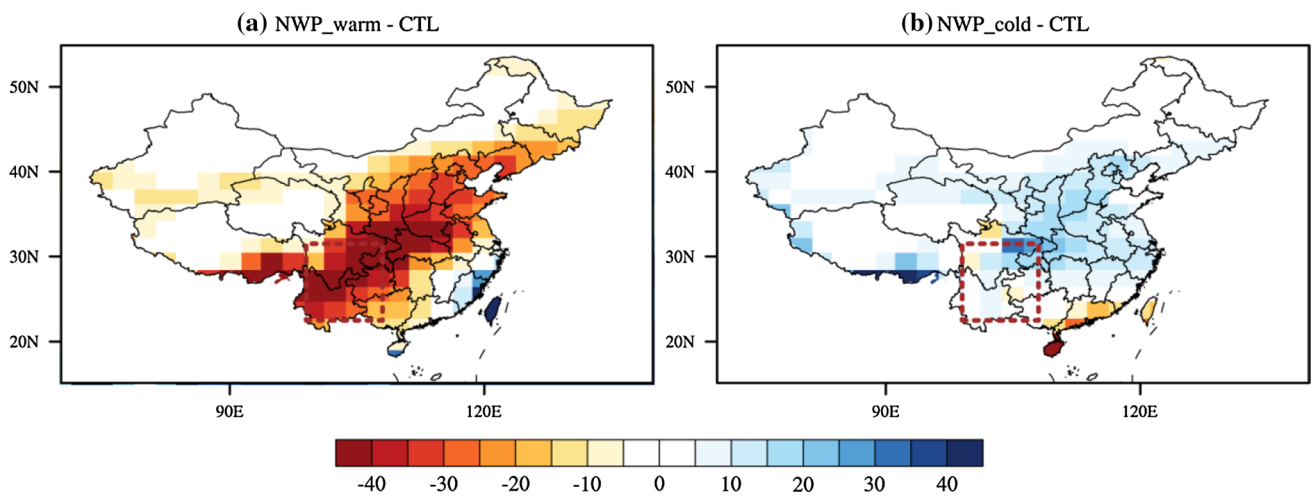

Fig. 11 NWP_warm (**a**)/NWP_cold (**b**) experiment minus control for autumn precipitation in China. Only statistically significant differences between NWP_warm and NWP_cold at 90 % confidence level are *plotted*
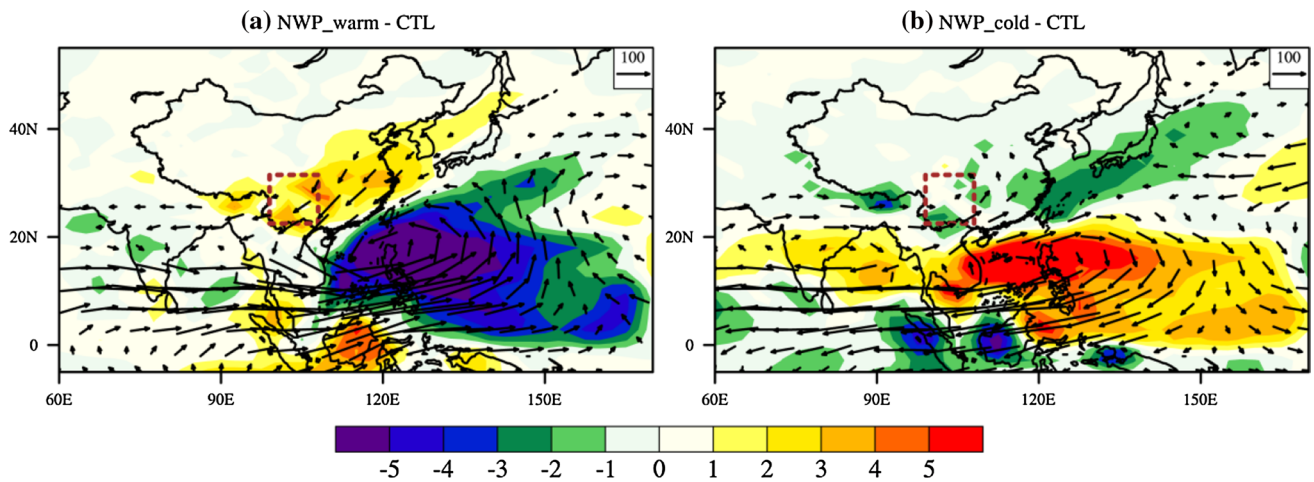
(a) NWP_warm - CTL   **(b)** NWP_cold - CTL

Fig. 12 The same as Fig. 11, but for vertically integrated water vapor flux (*vectors*, in units of kg s^{-1} m^{-1}) and moisture divergence (*shading*, 10^{-5} kg s^{-1} m^{-2})

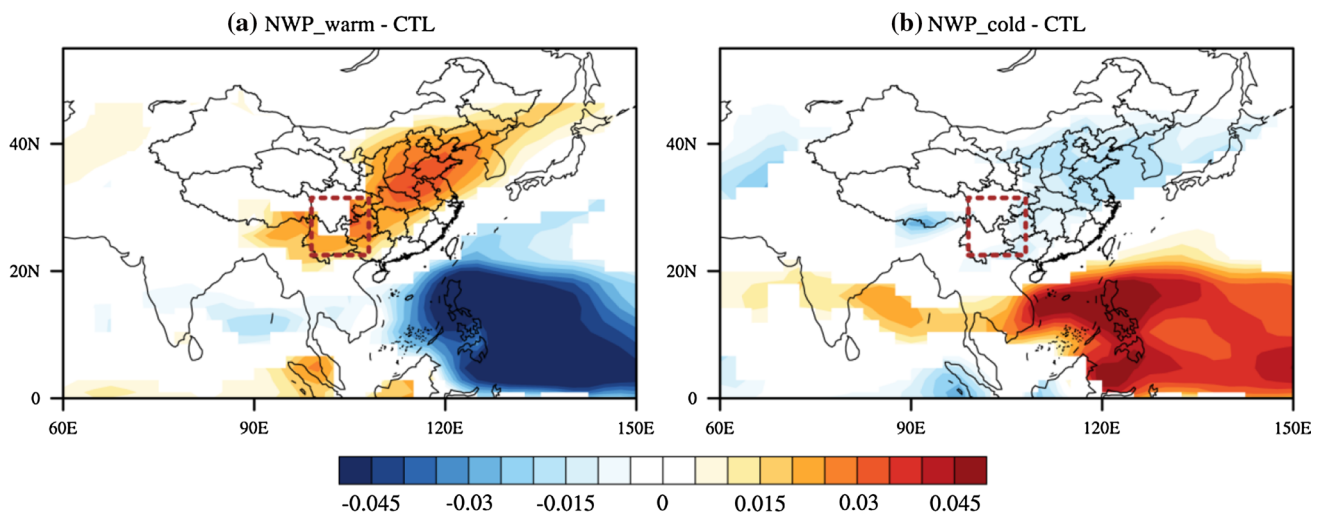**(a)** NWP_warm - CTL   **(b)** NWP_cold - CTL

Fig. 13 The same as Fig. 11, but for pressure vertical velocity at 500 h Pa (Pa s^{-1})

the presence of warm NWP SST, the AGCM simulates large-scale anomalous ascent (Fig. 13a) and upper-level divergence (Fig. 14a) in the NWP, with one path of the outflow heading northwestward and converging over SWC, which induces relative downward motion and suppression of convection. The opposite is true for the cold NWP SST configuration. Finally, it is noteworthy that the precipitation anomalies and atmospheric fields related to NWP warm and cold SST are asymmetric: the precipitation, moisture transport, and 500 h Pa velocity responses over SWC are weaker during NWP cold phases compared to NWP warm phases, probably due to nonlinear atmospheric responses to NWP SST. Despite the difference in amplitude, the broad patterns exhibit marked symmetric features. This type of asymmetry, thus, does not affect our conclusion.

In general, the results of the numerical experiments, forced by SST anomalies in the NWP region alone, are generally consistent with observational analysis. This therefore indicates that the statistical relationship derived from observation is a physically robust relation and that a strong contribution from NWP SST forcing drives precipitation variability in SWC.

3.4 Precursory signal

The concurrent SST-precipitation relation is important for understanding the dynamical process, but it has no significance for prediction. As shown in Fig. 3a, a strong relationship is found when SST leads autumn precipitation by one season. This spatial pattern is generally comparable to the
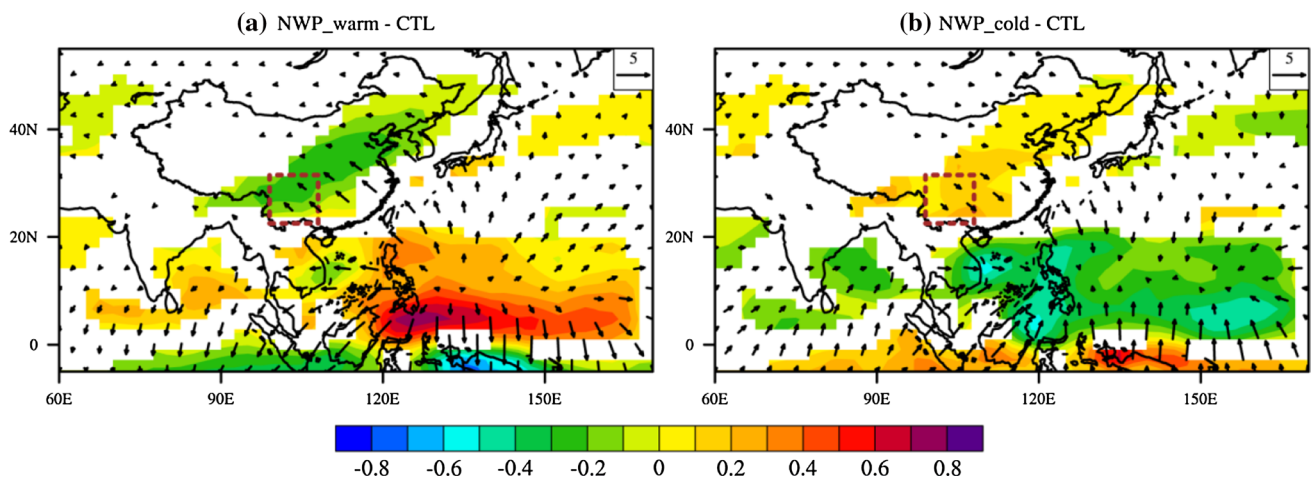
Fig. 14 The same as Fig. 11, but for 200 h Pa divergent winds (*arrows*, m s^{-1}) and divergence (*shading*, 10^{-5} s^{-1})
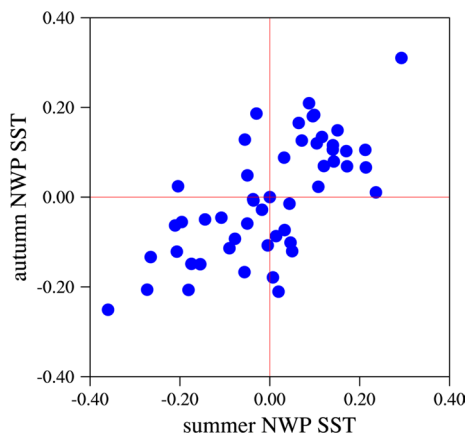

Fig. 15 *Scatter plot* of NWP SST anomalies in summer (x-axis) versus those in the following autumn (y-axis). Each *dot* corresponds to 1 year

simultaneous correlation map shown in Fig. 3b, implying that NWP SST anomalies in summer may provide significant signals for SWC drought in autumn. To substantiate this, Fig. 15, a scatter diagram of the NWP SST anomaly in autumn plotted against its value in the previous summer, is presented to measure whether the summertime NWP SST anomaly persists through the following autumn. During 1961–2011, 76 % of all cases fall into the top-right or bottom-left quadrant, reflecting the persistence of the state of NWP SST. It is probable that positive wind-evaporation-SST feedback acts to maintain the existing SST anomalies (Wang et al. 2000). From summer to autumn, the local positive/negative SST anomalies are accompanied by low-level anomalous easterlies/westerlies (Fig. 7), which weaken/strengthen southwesterly mean winds and give rise to reduced/enhanced wind speed (figure not shown). In response to reduced/enhanced wind speed, evaporation
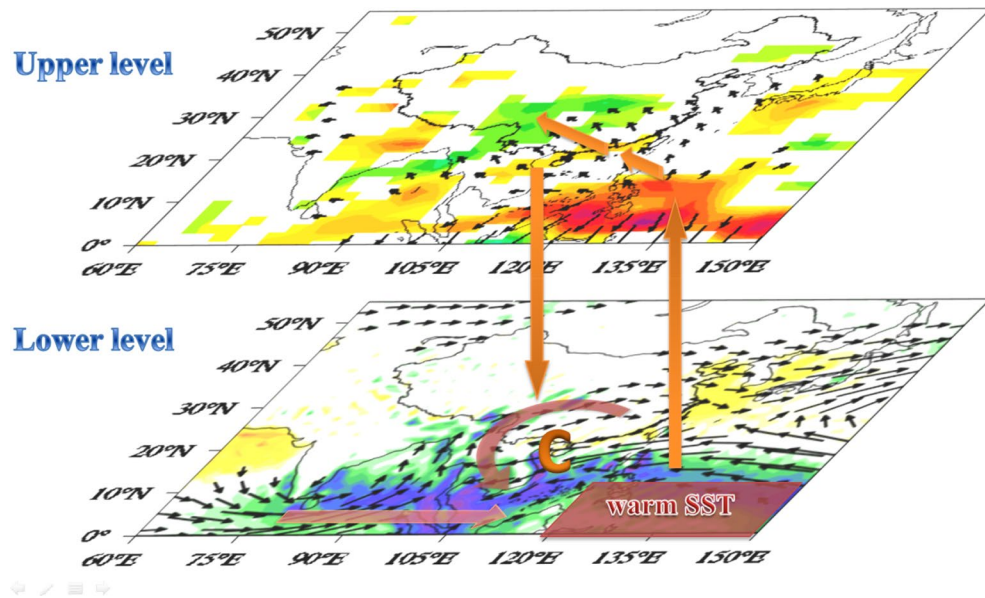
decreases/increases, contributing to the positive/negative SST persistence. Moreover, the warm-SST-related onshore wind anomalies (easterlies) suppress the oceanic mixing and upwelling and thereby help to maintain warmer SST, and vice versa. This result has two important implications: (1) NWP SST in summer has a predictive potential for SWC drought during the following autumn; and (2) because NWP SST is a persistent feature lasting from summer to autumn, it is likely to be a forcing to the atmospheric circulation rather than a response.

4 Conclusions

The causes of severe drought over SWC in autumn are investigated in detail based on grid rainfall, JRA-55 reanalysis, and ERSST data during 1961–2011. On the interannual timescale, the variation of SWC precipitation is highly negatively correlated with NWP SST in autumn. The dynamic processes linking drought in SWC to NWP SST anomalies are then explored.

Figure 16 illuminates the gross structure of the key ingredients of the circulation anomalies associated with SWC drought in response to a warm NWP. Three causal links are identified: (1) In the case of warm NWP SST, an anomalous cyclonic flow stretching across the South China Sea and its surroundings orients against the climatological moisture transport conveyor, which plays an important role in carrying abundant moisture from the NWP into SWC. Therefore, this cyclone causes a decrease in the moisture supply. (2) Warm NWP SST acts to intensify the zonal water vapor flux into the Indonesian region, but the poleward moisture transport into SWC decreases since most of the moisture is transferred to the maritime continent. (3) Warm NWP SST leads to rising air coupled with divergent

Fig. 16 Schematic diagram of the response of atmospheric circulation to NWP SST warming. The *black vectors* and *shaded area* in the *bottom panel* denote climatological moisture flux and its divergence (identical to Fig. 6); the *brown bold arrows* and *semicircle* schematically indicate the anomalous circulation induced by warm SST in the NWP

outflow in the upper level, with one branch of the currents converging in SWC and inducing sinking motion. These three features are unfavorable for precipitation formation in SWC. On the other hand, cold NWP SST fuels moisture convergence and plentiful precipitation in SWC.

In addition to statistical techniques, AGCM experiments are also carried out to actually describe the physical processes that connect NWP SST with SWC precipitation. These numerical experiments, forced by SST anomalies in the NWP region alone, resemble the observational analysis, confirming that a physical relation, rather than just an apparent statistical relation, does exist between NWP SST and SWC precipitation and that the anomalous atmospheric patterns arise to a large extent from NWP SST anomalies.
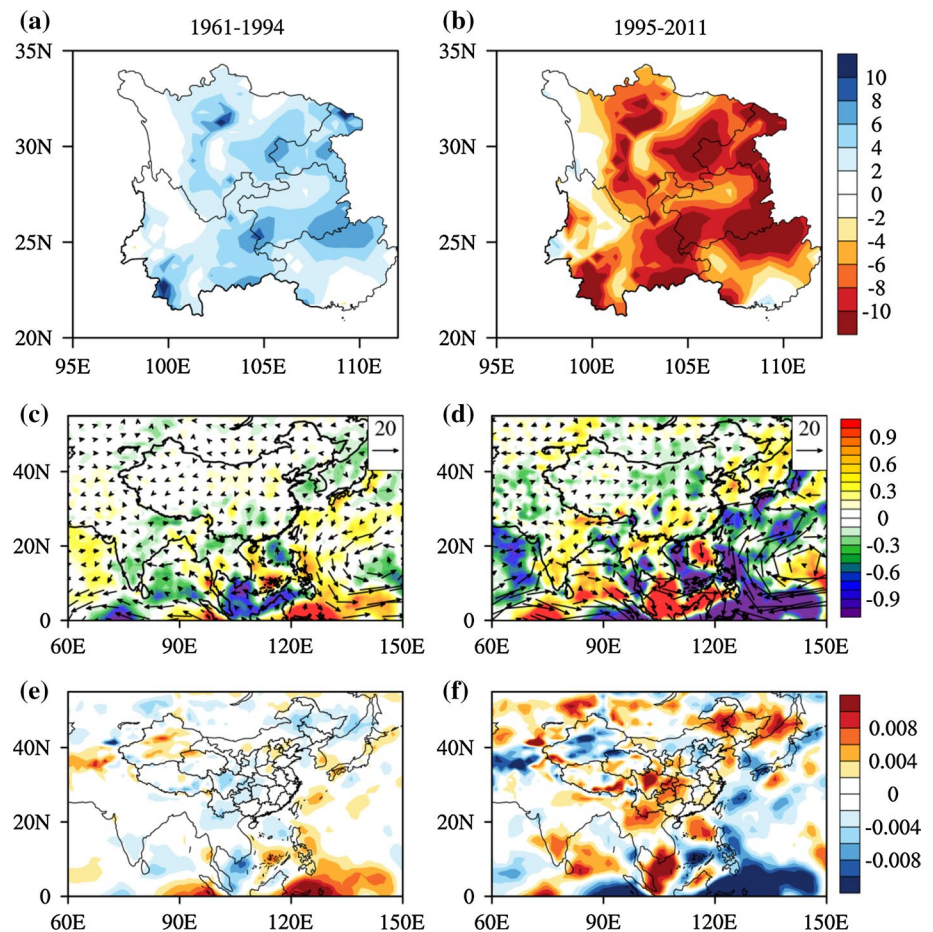
We show that autumn precipitation in SWC also has a negative correlation with NWP SST in the preceding summer, suggesting that summer NWP SST anomalies constitute an important precursory signal for autumn SWC precipitation. Consequently, this precursory signal will be helpful for advance decision making and mitigation.

5 Discussion

The variation of SWC precipitation exhibits not only inter-annual but remarkably interdecadal variability. In this section, we preliminarily investigate the corresponding decadal change of atmospheric circulation and propose a plausible cause. As shown in Fig. 4a, the SWC rainfall regime in autumn undergoes an abrupt shift in 1994, characterized by long-lasting precipitation deficits for approximately 15 years. This result is consistent with the observed evidence that SWC has suffered from frequent severe and

persistent droughts in recent decades. Figure 17a, b displays the spatial pattern of two rainfall regime shifts. On average, the autumn rainfall over SWC is 6–8 mm above normal during 1961–1994, whereas it is 10 mm lower than normal during recent decades. Linked to the decadal change of precipitation are the consistent changes in atmospheric circulation. After 1994, an anomalous cyclone prevails in the South China Sea region, along with significant intensification of zonal moisture transport along the equatorial Indian Ocean, which results in a deficient moisture supply and is therefore unfavorable for precipitation in SWC (Fig. 17c, d). Moreover, the anomalous downward motion also contributes to the decrease in precipitation in SWC after 1994 (Fig. 17e, f). Since the precipitation regime shift coincides well with a significant sudden change of NWP SST (see Sect. 3.1), which has been continuously warm in recent decades, and the patterns of atmospheric circulation for the two stable regimes (1961–1994 and 1995–2011) are analogous to those at the interannual timescale, it is speculated that the interdecadal variation of autumn precipitation in SWC is driven by the fundamental regime shifts in NWP SST. However, the reliability of this hypothesis should be studied further using statistical techniques and climate modeling. In addition, the decadal rainfall change over SWC around the mid-1990s may not be an isolated phenomenon, because similar shifts are found in summer precipitation over Eastern and Southern China and the onset of the South China Sea summer monsoon. For example, Ding et al. (2008) and Wu et al. (2010) both noticed that summer precipitation over Southern China experienced a significant increase around 1992/1993; Liu et al. (2011) and Li et al. (2012) both discuss the decadal summer rainfall shifts around the mid-1990s over Eastern China. Yuan and

Fig. 17 Spatial distribution of **a**, **b** autumn rainfall anomalies over SWC (unit: mm) **c**, **d** anomalous vertically integrated moisture transport (*vectors*, kg s^{-1} m^{-1}) and its divergence (*shading*, 10^{-5} kg s^{-1} m^{-2}), and **e**, **f** anomalous vertical velocity (unit: Pa s^{-1}) during 1961–1994 (*1st column*) and 1995–2011 (*2nd column*)

Chen (2013) investigated the roles of the tropical convective activities in the earlier onset of the summer monsoon after 1993. Therefore, more work is needed to understand the interdecadal change of autumn SWC precipitation.

Although here we investigate the physical mechanism by which NWP SST influences SWC precipitation in autumn, further studies are needed to reveal the causes of SWC drought in other seasons (i.e., summer and spring). In addition, since atmospheric circulation and precipitation anomalies are usually forced with certain SST anomaly patterns, we investigate the plausible role of SST in depth in this study. However, other possible impacting factors, such as the thermal conditions on the Tibetan Plateau, local land-air interaction, and high-latitude systems, should be explored in future work.

References

Barriopedro D, Gouveia CM, Trigo RM, Wang L (2012) The 2009/10 drought in China: possible causes and impacts on vegetation. J Hydrometeor 13:1251–1267

Chen W, Wang L, Xue Y, Sun S (2009) Variabilities of the spring river runoff system in East China and their relations to precipitation and sea surface temperature. Int J Climatol 29:1381–1394. doi:10.1002/joc.1785

Chen W, Feng J, Wu R (2013a) Roles of ENSO and PDO in the link of the East Asian Winter Monsoon to the following summer monsoon. J Clim 26:622–635

Chen W, Lan X, Wang L, Ma Y (2013b) The combined effects of the ENSO and the Arctic Oscillation on the winter climate anomalies in East Asia. Chin Sci Bull 58:1355–1362

Ding Y, Wang Z, Sun Y (2008) Inter-decadal variation of the summer precipitation in East China and its association with decreasing Asian summer monsoon. Part I: observed evidences. Int J Climatol 28:1139–1161

Ebita A, Kobayashi S, Ota Y, Moriya M, Kumabe R, Onogi K, Harada Y, Yasui S, Miyaoka K, Takahashi K (2011) The Japanese 55-year reanalysis "JRA-55": an interim report. Sola 7:149–152

Feng L, Li T, Yu W (2014) Cause of severe droughts in Southwest China during 1951–2010. Clim Dyn 43:2033–2042. doi:10.1007/s00382-013-2026-z

Gill AE (1980) Some simple solutions for heat-induced tropical circulation. Q J R Meteorol Soc 106:447–462

Huang G (2004) An index measuring the interannual variation of the East Asian summer monsoon—the EAP index. Adv Atmos Sci 21:41–52

Li Y, Xu H, Liu D (2009) Features of the extremely severe drought in the east of Southwest China and anomalies of atmospheric circulation in summer 2006. Acta Meteorol Sin 67:122–132

Li X, Wen Z, Zhou W, Wang D (2012) Atmospheric water vapor transport associated with two decadal rainfall shifts over East China. J Meteor Soc Jpn 90:587–602

Li X, Zhou W, Li C, Song J (2013) Comparison of the annual cycles of moisture supply over Southwest and Southeast China. J Clim 26:10139–10158

Liu Y, Huang G, Huang R (2011) Inter-decadal variability of summer rainfall in Eastern China detected by the Lepage test. Theor Appl Climatol 106:481–488

Lu E, Luo Y, Zhang R, Wu Q, Liu L (2011) Regional atmospheric anomalies responsible for the 2009–2010 severe drought in China. J Geophys Res Atmos 116:D21114

Qiu J (2010) China drought highlights future climate threats. Nature 465:142

Shang K, Zhan F, He J, Qi L (2014) Impact of the preceding-summer heat content over western Pacific warm pool on spring Persistent Rain and its possible meachanism. Acta Oceanol Sin 36(1):86–97 (in Chinese)

Smith TM, Reynolds RW, Peterson TC, Lawrimore J (2008) Improvements to NOAA's historical merged land–ocean surface temperature analysis (1880–2006). J Clim 21:2283–2296

Wang B, Wu R, Fu X (2000) Pacific-East Asian teleconnection: how does ENSO affect East Asian climate? J Clim 13:1517–1536

Wang YH, Chen W, Zhang JY, Nath D (2013) Relationship between soil temperature in May over Northwest China and the East Asian summer monsoon precipitation. Acta Meteor Sin 27(5):716–724

Wu R, Wen Z, Yang S, Li Y (2010) An interdecadal change in Southern China summer rainfall around 1992/93. J Clim 23:2389–2403

Yang J, Gong D, Wang W, Hu M, Mao R (2012) Extreme drought event of 2009/2010 over southwestern China. Meteor Atmos Phys 115:173–184

Ye T, Shi P, Wang J, Liu L, Fan Y, Hu J (2012) China's drought disaster risk management: perspective of severe droughts in 2009–2010. Int J Disaster Risk Sci 3:84–97

Yuan F, Chen W (2013) Roles of the tropical convective activities over different regions in the earlier onset of the South China Sea summer monsoon after 1993. Theor Appl Climatol 113:175–185

Zhang J, Jiang L, Feng Z, Li P (2012a) Detecting effects of the recent drought on vegetation in southwestern China. J Resour Ecol 3:43–49

Zhang L, Xiao J, Li J, Wang K, Lei L, Guo H (2012b) The 2010 spring drought reduced primary productivity in southwestern China. Environ Res Lett 7:045706

Zhang M, He J, Wang B, Wang S, Li S, Liu W, Ma X (2013a) Extreme drought changes in Southwest China from 1960 to 2009. J Geogr Sci 23:3–16

Zhang W, Jin FF, Zhao JX, Qi L, Ren HL (2013b) The possible influence of a non-conventional El Niño on the severe autumn drought of 2009 in Southwest China. J Clim 26:8392–8405

Zhou W, Chan JCL (2006) ENSO and the South China Sea summer monsoon onset. Int J Climatol 27(2):157–167

Zhou W, Li C, Chan JCL (2006) The interdecadal variations of the summer monsoon rainfall over South China. Meteor Atmos Phys 93:165–175

Zhou W, Chen W, Wang DX (2012) The implications of El Niño-Southern Oscillation signal for South China monsoon climate. Aquat Ecosyst Health Manag 15:14–19